Opto-mechanical artificial eye with accommodative ability

José J. Esteve-Taboada,[1,*] Antonio J. Del Águila-Carrasco,[1] Iván Marín-Franch,[1] Paula Bernal-Molina,[1] Robert Montés-Micó,[1] and Norberto López-Gil[2]

[1]*Optometry Research Group (GIO), Department of Optics, University of Valencia, Spain*
[2]*Vision Sciences Research Group (CiViUM), University of Murcia, Spain*
[*]*josejuan.esteve@uv.es*

Abstract: The purpose of this study was to describe the design and characterization of a new opto-mechanical artificial eye (OMAE) with accommodative ability. The OMAE design is based on a second-pass configuration where a small source of light is used at the artificial retina plane. A lens whose focal length can be changed electronically was used to add the accommodation capability. The changes in the OMAE's aberrations with the lens focal length, which effectively changes the accommodative state of the OMAE, were measured with a commercial aberrometer. Changes in power and aberrations with room temperature were also measured. The OMAE's higher-order aberrations (HOAs) were similar to the ones of the human eye, including the rate at which fourth-order spherical aberration decreased with accommodation. The OMAE design proposed here is simple, and it can be implemented in an optical system to mimic the optics of the human eye.

OCIS codes: (330.7326) Visual optics, modeling; (120.4880) Optomechanics; (120.4570) Optical design of instruments.

References and links

1. N. E. Norrby, "Standardized methods for assessing the imaging quality of intraocular lenses," Appl. Opt. **34**(31), 7327–7333 (1995).
2. P. G. Gobbi, F. Fasce, S. Bozza, and R. Brancato, "Optomechanical eye model with imaging capabilities for objective evaluation of intraocular lenses," J. Cataract Refract. Surg. **32**(4), 643–651 (2006).
3. A. Barcik, J. Nowak, D. Siedlecki, M. Zając, and J. Zarówny, "Physical model of human eye with implantable intraocular lenses," Proc. SPIE **7141**, 71411A (2008).
4. C. E. Campbell, "Wavefront measurements of diffractive and refractive multifocal intraocular lenses in an artificial eye," J. Refract. Surg. **24**(3), 308–311 (2008).
5. R. C. Bakaraju, K. Ehrmann, D. Falk, A. Ho, and E. Papas, "Physical human model eye and methods of its use to analyse optical performance of soft contact lenses," Opt. Express **18**(16), 16868–16882 (2010).
6. R. C. Bakaraju, K. Ehrmann, D. Falk, A. Ho, and E. Papas, "Optical performance of multifocal soft contact lenses via a single-pass method," Optom. Vis. Sci. **89**(8), 1107–1118 (2012).
7. D. Loshin and G. Fry, "Aberrations of spherocylindrical spectacle lenses," Am. J. Optom. Physiol. Opt. **53**(3), 124–136 (1976).
8. D. A. Heath, G. L. McCormack, and W. H. Vaughan, "Mapping of ophthalmic lens distortions with a pinhole camera," Am. J. Optom. Physiol. Opt. **64**(10), 731–733 (1987).
9. C. Zhou, W. Wang, K. Yang, X. Chai, and Q. Ren, "Measurement and comparison of the optical performance of an ophthalmic lens based on a Hartmann-Shack wavefront sensor in real viewing conditions," Appl. Opt. **47**(34), 6434–6441 (2008).
10. L. A. Carvalho, J. C. Castro, and L. A. Carvalho, "Measuring higher order optical aberrations of the human eye: techniques and applications," Braz. J. Med. Biol. Res. **35**(11), 1395–1406 (2002).
11. N. Sredar, H. Queener, C. Li, C. Ting, H. Hofer, and J. Porter, "Wavefront sensorless confocal adaptive optics scanning laser ophthalmoscopy in the human eye," J. Vis. **10**(15), 58 (2010).
12. S. Chiesa and J. C. Dainty, "Calibration and performance of a pyramid wavefront sensor for the eye," J. Mod. Opt. **59**(16), 1415–1427 (2012).
13. N. R. Dodaro and D. P. Maxwell, Jr., "An eye for an eye. A simplified model for teaching," Arch. Ophthalmol. **113**(6), 824–826 (1995).

#240874 Received 15 May 2015; revised 30 Jun 2015; accepted 30 Jun 2015; published 17 Jul 2015

14. L. Donovan, G. Brian, and R. du Toit, "A device to aid the teaching of retinoscopy in low-resource countries," Br. J. Ophthalmol. **92**(2), 294 (2008).
15. International Organization for Standardization, "ISO 11979-2:2014. Ophthalmic implants - Intraocular lenses - Part 2: Optical properties and test methods," (2014).
16. International Organization for Standardization, "ISO 11979-3:2012. Ophthalmic implants - Intraocular lenses - Part 3: Mechanical properties and test methods," (2012).
17. E. Moreno-Barriuso and R. Navarro, "Laser Ray Tracing versus Hartmann-Shack sensor for measuring optical aberrations in the human eye," J. Opt. Soc. Am. A **17**(6), 974–985 (2000).
18. E. J. Fernández and P. Artal, "Dynamic eye model for adaptive optics testing," Appl. Opt. **46**(28), 6971–6977 (2007).
19. R. A. Applegate, L. N. Thibos, M. D. Twa, and E. J. Sarver, "Importance of fixation, pupil center, and reference axis in ocular wavefront sensing, videokeratography, and retinal image quality," J. Cataract Refract. Surg. **35**(1), 139–152 (2009).
20. P. G. Gobbi, F. Fasce, S. Bozza, G. Calori, and R. Brancato, "Far and near visual acuity with multifocal intraocular lenses in an optomechanical eye model with imaging capability," J. Cataract Refract. Surg. **33**(6), 1082–1094 (2007).
21. A. Arianpour, E. J. Tremblay, I. Stamenov, J. E. Ford, D. J. Schanzlin, and Y. Lo, "An optomechanical model eye for ophthalmological refractive studies," J. Refract. Surg. **29**(2), 126–132 (2013).
22. N. Brown, "The change in shape and internal form of the lens of the eye on accommodation," Exp. Eye Res. **15**(4), 441–459 (1973).
23. A. J. Lang, V. Lakshminarayanan, and V. Portney, "Phenomenological model for interpreting the clinical significance of the in vitro optical transfer function," J. Opt. Soc. Am. A **10**(7), 1600–1610 (1993).
24. M. S. Millán Garcia-Varela, F. Alba Bueno, and F. Vega Lerín, Experiment design for through-focus testing of intraocular lenses" in Proc. SPIE 8785, 8th Iberoamerican Optics Meeting and 11th Latin American Meeting on Optics, Lasers, and Applications, 8785CP.M. F. Martins Costa, ed. (SPIE, 2013).
25. J. S. Pepose, D. Wang, and G. E. Altmann, "Comparison of through-focus image sharpness across five presbyopia-correcting intraocular lenses," Am. J. Ophthalmol. **154**(1), 20–28 (2012).
26. M. Sheehan, A. Goncharov, and C. Dainty, "Design of a versatile clinical aberrometer" in Proc. SPIE 5962, Optical Design and Engineering II, 59620M.L. Mazuray and R. Wartmann, eds. (SPIE, 2005).
27. A. G. Optotune, "Fast Electrically Tunable Lens. EL-10-30-Series Datasheet," http://www.optotune.com/images/products/Optotune%20EL-10-30.pdf.
28. M. Curtis and F. Farago, Handbook of Dimensional Measurement (Industrial Press, 2013).
29. N. Visser, T. T. Berendschot, F. Verbakel, A. N. Tan, J. de Brabander, and R. M. Nuijts, "Evaluation of the comparability and repeatability of four wavefront aberrometers," Invest. Ophthalmol. Vis. Sci. **52**(3), 1302–1311 (2011).
30. L. N. Thibos, X. Hong, A. Bradley, and R. A. Applegate, "Accuracy and precision of objective refraction from wavefront aberrations," J. Vis. **4**(4), 329–351 (2004).
31. P. B. Kruger and J. Pola, "Stimuli for accommodation: blur, chromatic aberration and size," Vision Res. **26**(6), 957–971 (1986).
32. P. B. Kruger, S. Mathews, K. R. Aggarwala, D. Yager, and E. S. Kruger, "Accommodation responds to changing contrast of long, middle and short spectral-waveband components of the retinal image," Vision Res. **35**(17), 2415–2429 (1995).
33. P. B. Kruger, N. López-Gil, and L. R. Stark, "Accommodation and the Stiles-Crawford effect: theory and a case study," Ophthalmic Physiol. Opt. **21**(5), 339–351 (2001).
34. N. López-Gil and R. Montés-Micó, "New intraocular lens for achromatizing the human eye," J. Cataract Refract. Surg. **33**(7), 1296–1302 (2007).
35. J. W. Goodman, Introduction to Fourier Optics (Roberts & Company Publishers, 2005).
36. M. Gu, Advanced Optical Imaging Theory (Springer-Verlag, 2000).
37. T. O. Salmon and C. van de Pol, "Normal-eye Zernike coefficients and root-mean-square wavefront errors," J. Cataract Refract. Surg. **32**(12), 2064–2074 (2006).
38. H. Cheng, J. K. Barnett, A. S. Vilupuru, J. D. Marsack, S. Kasthurirangan, R. A. Applegate, and A. Roorda, "A population study on changes in wave aberrations with accommodation," J. Vis. **4**(4), 272–280 (2004).
39. N. López-Gil and V. Fernández-Sánchez, "The change of spherical aberration during accommodation and its effect on the accommodation response," J. Vis. **10**(13), 12 (2010).
40. N. López-Gil, V. Fernández-Sánchez, R. Legras, R. Montés-Micó, F. Lara, and J. L. Nguyen-Khoa, "Accommodation-related changes in monochromatic aberrations of the human eye as a function of age," Invest. Ophthalmol. Vis. Sci. **49**(4), 1736–1743 (2008).

1. Introduction

Opto-mechanical artificial eyes (OMAEs) imitate the basic image formation of a human eye, and are mainly used for the in-vitro test of the optical performances of refractive correction devices such as intraocular [1–4], contact [5,6], or ophthalmic [7–9] lenses. OMAEs are also

#240874 Received 15 May 2015; revised 30 Jun 2015; accepted 30 Jun 2015; published 17 Jul 2015

used in the calibration of optical systems, for instance as test beds for measuring and characterizing the optical wavefront [10–12], and to practice clinical refraction [13,14].

There are two main configurations, which depend on the purpose of the OMAE: the single- and the double-pass configuration. In the single-pass configuration the aerial image is directly recorded in the image space after the light passes through the optics of the OMAE. This configuration can also be called first-pass configuration and is an international ISO standard method to test refractive correction lenses, including intraocular lenses (IOLs) and contact lenses (CLs) [15,16]. Nevertheless, with this configuration the optical wavefront cannot be characterized. In the double-pass configuration, the light passes through the optics of the OMAE, hits an artificial retina that diffuses and reflects it towards the object space, where the image is recorded. This configuration is commonly used as test bed for optical wavefront characterization, where a wavefront sensor is properly conjugated with the OMAE. In some double-pass configurations, a rotating diffuser acting as the artificial retina is used to break laser temporal coherence, producing thus an incoherent image after the second pass through the OMAE optics [17,18].

The double-pass configuration has the practical limitation that specular reflections occur in the different refractive surfaces, which can severely affect wavefront measurements. Techniques to avoid these reflections include shifting the incoming beam to prevent undesirable reflections from reaching the wavefront sensor [19]. Yet, two problems remain. The first one is that optics with small pupils cannot be tested. The second is that an image may be formed outside of the iso-planatism area after the first pass in an ametropic OMAE so the aberrations measured after the second-pass do not correspond to the on-axis aberrations. Another limitation of common double-pass configurations is that OMAEs have fixed optical power. Therefore, to form sharp images of objects placed at different distances their axial length should be modified [20], or diverse lenses should be added [21]. This fact represents an important difference with respect to the strategy used by the human eye during accommodation [22]. And its results have to be carefully interpreted, since when the OMAE's axial length is modified or a lens is added in front of it, there is a greater change in the size of the retinal image than that of the human eye, and a greater change in its point-spread function (PSF) [23–25].

In this work, we built and tested a new OMAE that includes two principal new features: a nearly punctual light source in the center of the artificial retina and a variable optical power lens to collimate the light beam or change its focus at different vergences from the OMAEs exit pupil. The key advantage of this second-pass configuration is that the OMAE can be used to reproduce any refractive or accommodative state as it does the human eye. An additional advantage of the proposed configuration is that it ensures that no undesirable reflections reach the wavefront sensor.

2. Materials and methods

2.1 Artificial eye design with accommodative ability

The proposed configuration is described following the sense of the propagation of light from the artificial retina plane. A near infrared (NIR) light emitting diode (LED) (TSHG6200, Vishay Intertechnology Inc., Malvern, PA, USA) with a wavelength of 850 nm is used together with a diffuser and an iris diaphragm centered with respect to the rest of the OMAE's optical components. A variable power source is used to feed the NIR LED that allows adjustment of the light intensity of the active retina. The diaphragm was fixed to 1-mm diameter that produces a geometrical angular size of 0.8°. This value is smaller than the angular size of the beacon used by standard eye aberrometry [26], and enough for the purpose of our experiments.

Changes in refractive state of the OMAE are achieved with the use of a lens with an electronically variable focal length (EL-10-30-NIR-LD, Optotune AG, Dietikon,

#240874 Received 15 May 2015; revised 30 Jun 2015; accepted 30 Jun 2015; published 17 Jul 2015

Switzerland). This tunable lens is filled with an optical fluid and sealed off with an elastic polymer membrane [27]. The OMAE's optical power is proportional to the pressure in the fluid, which is modulated by an electromagnetic actuator that responds to the electrical current applied. To select the electrical current we used the electrical driver and software provided by the manufacturer of the tunable lens.

A second diaphragm iris (artificial pupil) was added just after the variable lens (about 1 mm away from its back surface). This iris acts as the aperture diaphragm of the OMAE. The diameter of this diaphragm can be adjusted manually from 1 mm to 8.5 mm. It simulates the effect of the iris in the human vision system.

Since the polymer membrane in the lens is elastic, its shape is influenced by gravity [27], which can induce a vertical coma of 0.3μm for a 5 mm pupil. To avoid that, the OMAE was designed to keep the lens horizontal. A 45°mirror was placed at 30 mm from the artificial pupil to fold the light 90° in order to have a horizontal beam exiting the OMAE. Figure 1 shows a three-dimensional rendering of the OMAE designed in this paper. To ensure a compact design, standard optical elements were used from the Linos Microbench series (Qioptiq Photonics GmbH, Munich, Germany).

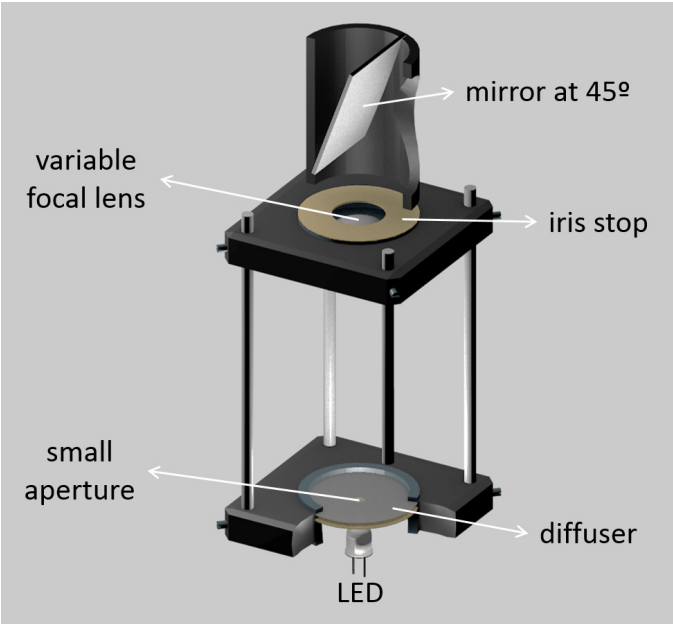

Fig. 1. Three-dimensional rendering of the OMAE designed.

2.2 Optical performance of the OMAE

The change in the electrical current drives the tunable lens a range in optical power from 7 D to 24 D. The distance between the artificial retina and the back surface of the tunable lens was set to 70 mm, so that the OMAE emmetropization point was in the middle of the total power interval of the tunable lens. By means of this configuration a large range of non-emmetropic eyes, as well as different dynamic accommodative behaviors, can be simulated. The precise electrical current necessary to achieve an emmetropic OMAE for a wavelength of 850 nm was found by an auto-collimation technique [28].

To characterize the aberrations and the dynamic behavior of the OMAE, a commercial aberrometer was used (irx3, Imagine Eyes, Orsay, France).It consists of a Shack-Hartmann wavefront sensor aberrometer, which shows high repeatability of total ocular aberrations [29]. The software of the aberrometer was used to get dynamic measurements of the wavefront. OMAE's wavefronts for different electrical currents applied to the tunable lens were obtained.

#240874 Received 15 May 2015; revised 30 Jun 2015; accepted 30 Jun 2015; published 17 Jul 2015

At the current that made the eye perfectly emmetropic, the defocus shown by the aberrometer corresponded to the chromatic difference between the wavelength used by the OMAE (850 nm) and that of the apparatus (780 nm, not used during the measurements) plus the internal defocus corrections used by the aberrometer to bring the wavefront data to a visible light.

2.3 Experiments

Three experiments were performed with the OMAE. First, we obtained the variations in refractive state and higher-order aberrations (HOAs) as a function of the electrical current applied to the tunable lens. Refractive state was computed by minimizing the variance of the wavefront [30]. Second, the dynamic variations in the OMAE's Zernike defocus term were obtained with both sinusoidal and rectangular profiles in the applied electrical current. Third, wavefront changes with temperature were assessed. Except for the third experiment, wavefront measurements were obtained at a room temperature of (21 ± 1) °C. All wavefront data was analyzed for a 5-mm pupil. Before starting with these experiments, repeatability tests were performed in the commercial wavefront sensor taking 20 independent measurements of the OMAE stabilized in the emmetropic state. These tests showed that the root mean square (RMS) of individual Zernike coefficients was below 0.01 μm.

3. Results

Figure 2 shows the result obtained in the first study. The electrical current variations in the tunable lens changed only its spherical power (variations obtained in the cylinder measurements were always below 0.1 D). The OMAE response was well described by a linear model, thus, $y = -0.05x + 6.20$, where x denotes the electrical current applied to the tunable lens in mA, and y the refractive state of the OMAE in D. This linear model described the OMAE behavior up to currents equal to 280 mA. For currents greater than 280 mA there were no changes in the optical power of the lens.

Figure 3 shows the changes in spherical aberration (SA), trefoil, and coma Zernike coefficients as a function of the electrical current applied to the tunable lens. The changes of the RMS corresponding to the third-order trefoil, third-order coma, and fourth-order SA were all below 0.1 μm.

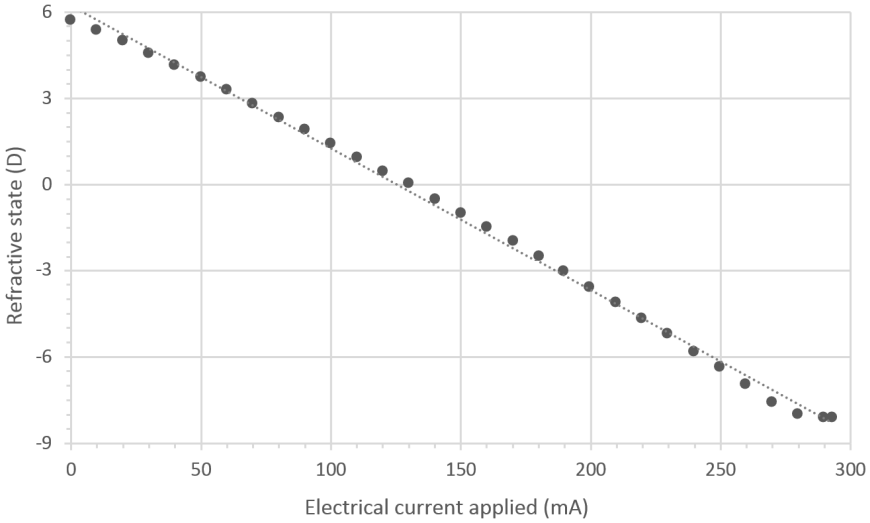

Fig. 2. Change in the OMAE's refractive state with the electrical current applied to the variable lens. Maximum standard deviation value was 0.01 D. Dashed line shows the linear model that best describes the OMAE response, $y = -0.05x + 6.20$, x being the electrical current applied to the tunable lens in mA, and y being the refractive state of the OMAE in D.

#240874 Received 15 May 2015; revised 30 Jun 2015; accepted 30 Jun 2015; published 17 Jul 2015

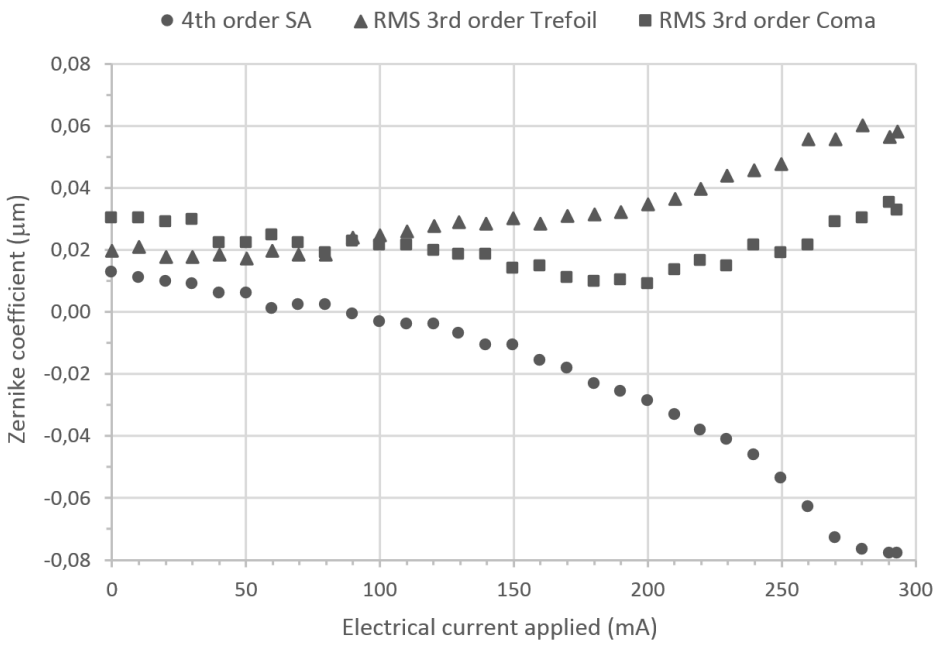

Fig. 3. Changes in the OMAE's higher-order aberrations with the electrical current applied to the variable lens: RMS for third-order trefoil (triangles); RMS for third-order coma (squares); and fourth-order spherical aberration (circles).

In the second experiment, the calibration line in Fig. 2 was used to modulate the current and generate a sinusoidal dynamic accommodation profile from 1 D to 3 D at a temporal frequency of 0.05 Hz. Those parameters were chosen because they are the values typically used in dynamic accommodation experiments for the human eye [31–33]. Figure 4(a) shows the variation in the OMAE's Zernike defocus term as a function of time. The peak-to-peak amplitude of the measured signal was lower or equal to the required one by around 0.15 D, which represents a decrease in the peak-to-peak amplitude of about 7.5%. Figure 4(b) shows the results obtained when the electrical current varied between 0 and 250 mA, to test the whole dynamic range of the tunable lens, at a frequency of 0.05 Hz following a square wave. The theoretical refractive change should be between + 5.70 D and −6.40 D (see Fig. 2), but the real peak-to-peak amplitude obtained was around 0.8 D smaller (0.6 D lower in the upper limit and 0.2 D in the lower limit). This reduction in the peak-to-peak amplitude represents a decrease of about 6.5%.

#240874 Received 15 May 2015; revised 30 Jun 2015; accepted 30 Jun 2015; published 17 Jul 2015

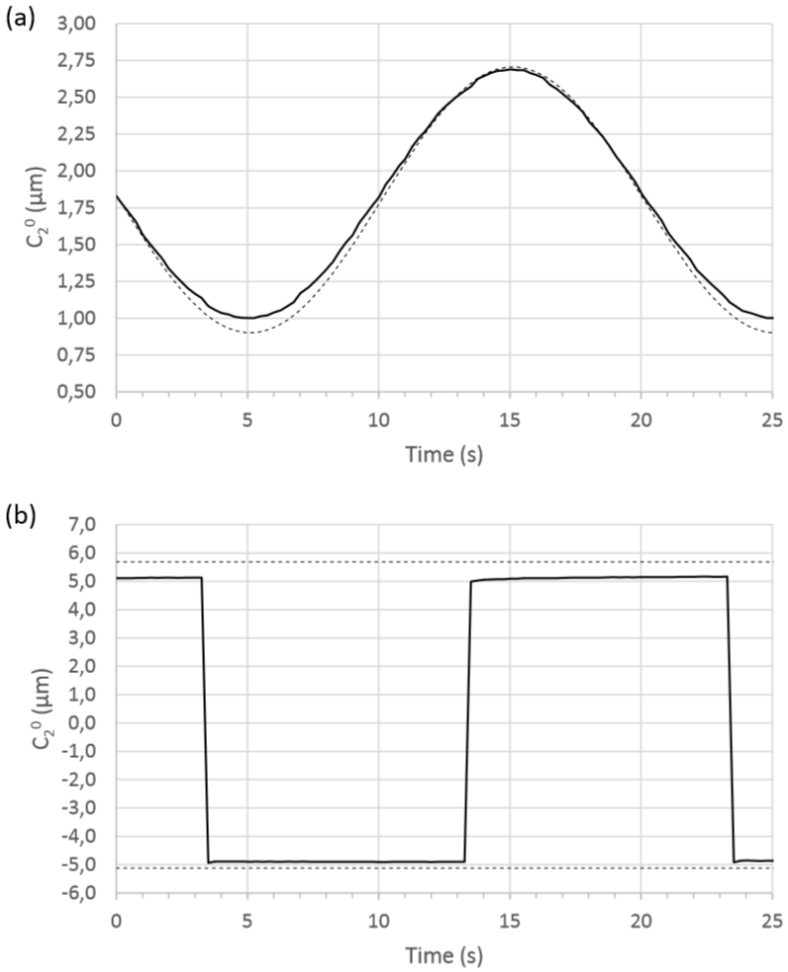

Fig. 4. (a) Zernike defocus coefficient for a sinusoidal change of the electrical current applied (0.05 Hz temporal frequency). Solid lines show measurements and dashed lines show the expected theoretical response. (b) Zernike defocus coefficient for a square wave change of the electrical current applied (0.05 Hz temporal frequency). Solid lines show measurements and dashed lines show the expected upper and lower limits.

In the third experiment, the temperature was increased from 15°C to 25°Cand measurements were taken every 30 minutes. The results showed that: defocus varied at a rate of −0.03 µm/°C ;astigmatism RMS at a rate of −0.04 µm/°C; while any of the other higher-order Zernike coefficients variations were less than 0.002 µm/°C.

4. Discussion

In contrast to the current OMAEs based on a first- or double-pass configuration, we have proposed a second-pass configuration artificial eye. This type of configuration presents an important practical advantage: wavefront can be easily obtained using an external independent aberrometer, avoiding the specular reflections of the incoming beam in the different refractive surfaces of the OMAE. These non-desired reflections may limit the measurements in a double-pass configuration unless they are removed, for instance, by shifting the incoming beam [19], although the potential problem that the aberrations measured after the second-pass do not correspond to the on-axis aberrations remains. The intensity of the NIR LED placed at the OMAE's artificial retina can be changed in order to get proper

#240874 Received 15 May 2015; revised 30 Jun 2015; accepted 30 Jun 2015; published 17 Jul 2015

measurements depending on the wavefront sensor used. The OMAE can serve to measure any optical element, such as IOLs, if they are introduced near the artificial pupil in a wet-cell. The wavefront of any optical element can, thus, be obtained as the difference between measured wavefronts with and without the optical element. If the optical element to be tested varies its optical power, these changes can be controlled by the OMAE's variable lens. That is, the variable lens can be changed so that the light exiting the OMAE is collimated.

There are other potential optical features that can be implemented with this type of optical configuration. For instance, the wavelength of the light source used in the OMAE can be changed in order to obtain the optical dispersion data of an optical element to be tested (CL or IOL). IOLs designed with longitudinal chromatic aberration to, e.g. correct that of the eye [34], can also be assessed with the OMAE. The physical diameter of the point source at the OMAE's retina may also be changed with a small pinhole to obtain a real PSF (including dispersion), instead of the low-pass frequency version obtained with a larger source (i.e. 1 mm) [35]. Speckle produced by a small coherent point source may be reduced by decreasing the intensity of the source at the retina and allowing a longer exposure time when the OMAE is working in a dynamic regime.

The variable lens can be used also to analyze simple dynamic accommodative responses, with, e.g., smooth continuous changes or fast steep transitions between two well-defined accommodative states. The results obtained in the proposed OMAE (see Fig. 4) demonstrate the high dynamic repeatability of the tunable lens. Nevertheless, the amplitude of the measured signal is always lower or equal to the expected one, and this difference depends on the amplitude of the profile function that defines the response required in the tunable lens. When the lens is driven by a sinusoidal profile (Fig. 4(a)), and for the low temporal frequency that was considered (0.05 Hz), the lens is able to increase its optical power to get a refraction in the OMAE of −3 D, but it is not able to be completely relaxed to get a refraction of −1 D.

Higher temporal frequencies were also tested (0.1 and 0.2 Hz). For these frequencies the behavior was the opposite. The lens was able to be relaxed to get −1 D of refraction in the OMAE, but it failed when increasing its power to get a refraction of −3 D. Similar behavior was obtained when driving the tunable lens with a square wave electrical current profile. This behavior may be explained by several parameters, such as the elasticity of the polymer membrane that models the lens, the hydrodynamic properties of the liquid that fills the polymer membrane, and the electrical characteristics of the operating driver. Nevertheless, errors in dynamic current-induced refractive state can be overcome by defining a greater upper limit and a smaller lower limit in the sinusoidal profile. As the dynamics of the lens are highly repeatable and the small differences in theoretical versus measured accommodative profiles fixed, the OMAE does not exhibit a hysteresis-like behavior, providing a very useful research tool for studies of the dynamic accommodative response of the human visual system.

The two main limitations of the OMAE are the presence of inherent HOAs and changes in low-order aberrations with temperature. Inherent HOAs (see Fig. 3) are far from the Maréchal criterion corresponding to an aberration-free system (RMS<λ/14) [36]. These inherent OMAE's HOAs cannot be avoided, although they can be characterized and, e.g., subtracted from IOL measurements, afterwards. Nevertheless, OMAE's RMS for the different HOAs for a 5 mm pupil are similar or even lower than that found in a non-pathological eye [37].In general, the changes in the OMAE's HOAs when varying its optical power are small except for the SA. Coincidentally, as the OMAE increases its optical power, the fourth-order SA decreases (see Fig. 3) in a similar fashion as it does for the human eye during accommodation [38]. The reason of this concordance may be due to the fact that the OMAE is using a similar procedure to increase its power to the one present in the human eye, and in both cases the surfaces of the variable lens had a negative asphericity (K<0) [39]. Nevertheless, the rate of decrease of fourth-order SA per diopter of refractive change obtained in the OMAE was lower than the one found in the human eye: 0.007 μm/D in the OMAE for 5 mm pupil, and 0.011 μm/D in the human eye for 4 mm pupil [40]. Nevertheless, it is important to keep in

#240874 Received 15 May 2015; revised 30 Jun 2015; accepted 30 Jun 2015; published 17 Jul 2015

mind that the total power of the OMAE is smaller than that of the human eye. For a voltage of about 130 mA, the OMAE proposed is emmetropic (Fig. 2), and its fourth-order SA is negative (Fig. 3). That does not agree with the human eye behavior, which usually presents a positive fourth-order SA at its relaxed state [37]. Then, for a more realistic imitation of the human eye, the OMAE should use an extra positive lens (acting as an artificial cornea) that increases the total power of the OMAE and give a positive fourth-order SA value [37,38].

As mentioned, the second limitation of the OMAE is that aberrations change with temperature. These changes are due to the thermal characteristics of the polymer membrane of the variable lens and the liquid filling the membrane. As temperature increases the liquid inside the membrane expands its volume increasing the power of the OMAE [27]. This change affects mainly the low-order aberrations of the artificial eye (defocus and astigmatism). Nevertheless, if room temperature cannot be controlled, it is possible to characterize these changes with temperature and take them into account later in data processing.

As a conclusion, in this work we have designed and tested an OMAE with two main new features. First, the OMAE includes an active retina, which permits the use of a second-pass configuration instead of the classical double-pass one, avoiding thus the non-desired reflections in the OMAEs optical surfaces. Second, the OMAE uses a variable optical power lens, which can be driven electronically, that allows for mimicking the optics of the human eye.

Acknowledgments

This research was partially supported by the European Research Council to R. Montés-Micó from the following grants: Starting Grant ERC-2012-StG-309416 from; Grant 15312/PI/10 from FundaciónSéneca (Región de Murcia), Spain, to N. López-Gil; research stay grant BEST/2014/107 from the Generalitat Valenciana to J.J. Esteve-Taboada; and research scholarship grant Atracció de Talent (UV-INV-PREDOC14-179135) from the Universidad de Valencia to Antonio J. Del Águila-Carrasco.

#240874 Received 15 May 2015; revised 30 Jun 2015; accepted 30 Jun 2015; published 17 Jul 2015